Schweizerischer Erdbebendienst
Service Sismologique Suisse
Servizio Sismico Svizzero
Swiss Seismological Service

ETH
Eidgenössische Technische Hochschule Zürich
Swiss Federal Institute of Technology Zurich

SITE CHARACTERIZATION REPORT

SLIES: Liestal (BL)

Dario Chieppa, Manuel Hobiger, Donat Fäh

Last Modification: 19th October, 2021

Schweizerischer Erdbebendienst (SED)
Service Sismologique Suisse
Servizio Sismico Svizzero
Servizi da Terratrembels Svizzer
ETH Zürich
Sonneggstrasse 5
8092 Zürich
Schweiz
dario.chieppa@sed.ethz.ch

Contents

Summary

Liestal (BL) is a city located in northern Switzerland about 10 km south-east from the city of Basel. The place was chosen as site for the installation of a new station, called SLIES, as part of the renewal project of the Swiss Strong Motion Network (SSMNet). In order to better assess the local subsurface, a passive seismic array was performed around the location of seismic station SLIES.

Most of the horizontal-to-vertical spectral ratio (H/V) curves show two peaks: the first one at about 1.0 Hz is interpreted as the fundamental peak, while the second one is located between 5.8 and 6.6 Hz and is interpreted as the first higher mode. At two locations, the first higher mode H/V peak was identified at 7.2 and 9.8 Hz.

The inversion of the passive seismic array measurements allows the estimation of the velocity profiles down to 350 m. Using velocity profiles with 3, 5, 7, 9 layers over the half-space or a profile with layers of fix thickness, two main interfaces are distinguished at about 1.5 and 18.5 meters. The basement with S-wave velocity ranging between 1843 and 2020 m/s is located at about 245–265 meters.

The V_{S30} value of the site is around 708.7 m/s, corresponding to soil class B in EC8 and SIA261. The theoretical shear-wave transfer functions from the retrieved V_S profiles predict an amplification function in good agreement with the empirical function recorded at station SLIES.

1 Introduction

The station SLIES is part of the Swiss Strong Motion Network (SSMNet). The station was installed on 18 September 2020 in the framework of the second phase of the Swiss Strong Motion Network (SSMNet) renewal project (Fig. 1). In order to better characterize the underground, to estimate the fundamental frequency of the site and the shear wave velocity, a passive array measurement was carried out on 29 June 2021.
The site is of interest for (i) its location close to Baselland hospital, for (ii) the proximity with the city of Basel and for (iii) the possibility to improve the network coverage in northern Switzerland. From a geological point of view, Liestal is located on gravels and fluvioglacial sediments of Late Pleistocene age overlying Mesozoic evaporite rocks (Fig. 2).

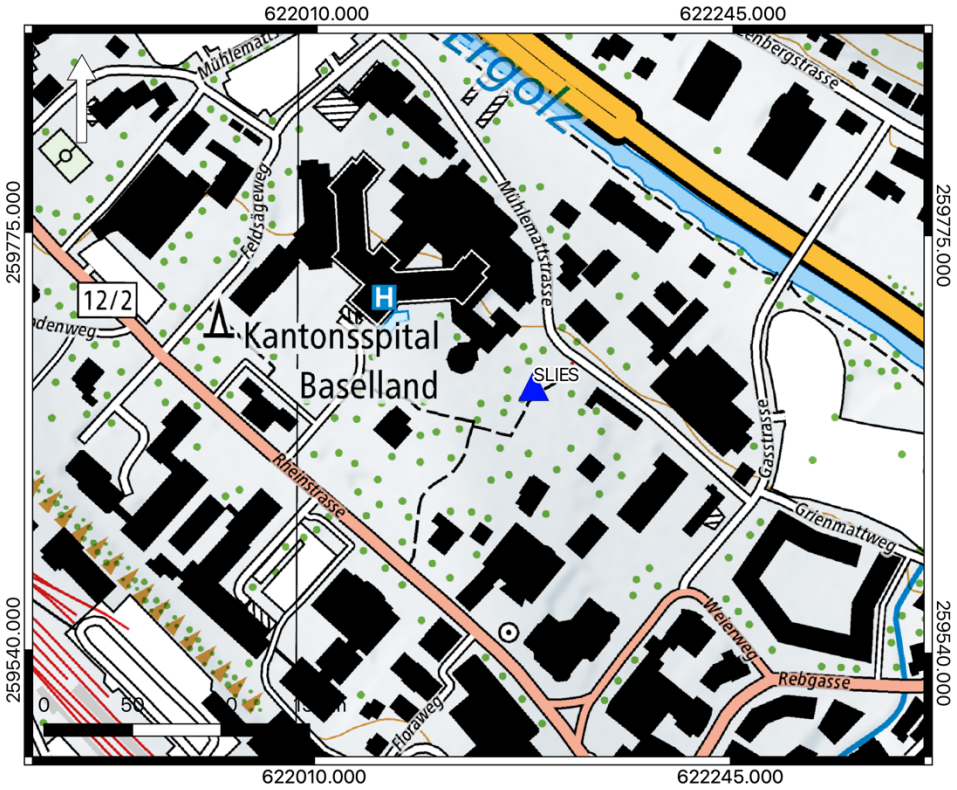

Figure 1: Map showing the location of the strong motion station (blue triangle) in Liestal. Source: Federal Office of Topography.

2 Geological setting

A geological map of the surroundings of Liestal is shown in Fig. 2: the red dots represent the location of the passive array measurement, while the blue triangle shows the location of station SLIES. The sensors deployed in June 2021 are located on alluvial sediments of Holocene age and on gravels and glaciofluvial sediments (Late Pleistocene). The station SLIES is located on gravels and glaciofluvial sediments.

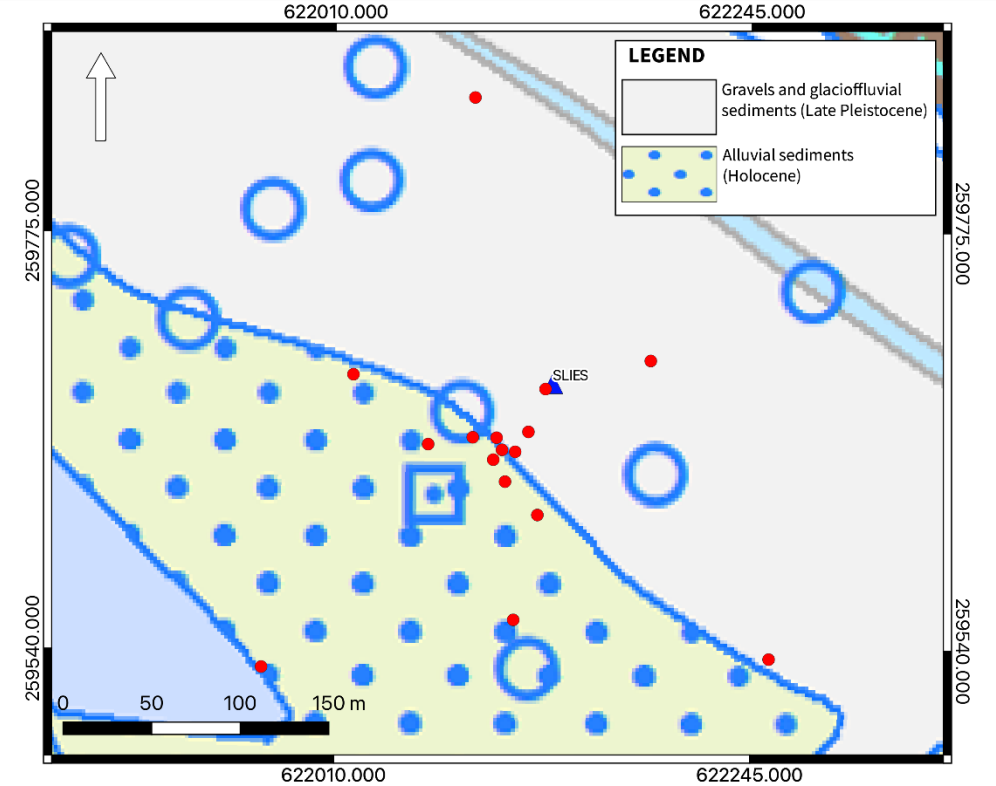

Figure 2: Geological map of the Liestal area. The stations of the passive array recordings are indicated by red triangles, whereas the position of the strong-motion station SLIES is shown by a blue triangle. Source: Federal Office of Topography.

3 Passive site characterization measurements

3.1 Data set

To characterize the deep underground structure around the seismic station, a passive seismic measurement was performed on 29 June 2020.

A single array of 16 stations was installed (Fig. 4). The stations were planned to be located on five rings of different radii around a central station. The three stations of each ring were planned to be rotated at about 120 degrees one from the other. The radii of the rings are 7.5, 18, 45, 95 and 200 meters. The array central station (LIES64) is located about 50 m south-west from station SLIES. Each ring, starting from the second, was rotated anticlockwise with respect to the inner ring of 44, 20, -24 and 63 degrees.

Each station consisted of a Lennartz 5s sensor connected to a Centaur digitizer, with the exception of four stations in the central part which had two sensors connected to the same digitizer. The station names of the array are composed of "LIES" followed by a two-digit number between 42 and 49, 52 and 55, 64, 65, 67 and 68 (corresponding to the Centaur digitizer serial number for numbers lower than 60 plus 20 to distinguish the use of the second channel). The array recording time was 150 minutes (9000s). The station locations were measured by a differential GPS system (Leica Viva GS10) which was set up to measure with a precision better than 5 cm. The coordinate points were acquired with a precision of a few centimeters.

Figure 3: Seismic station installation example for the measurements in Liestal.

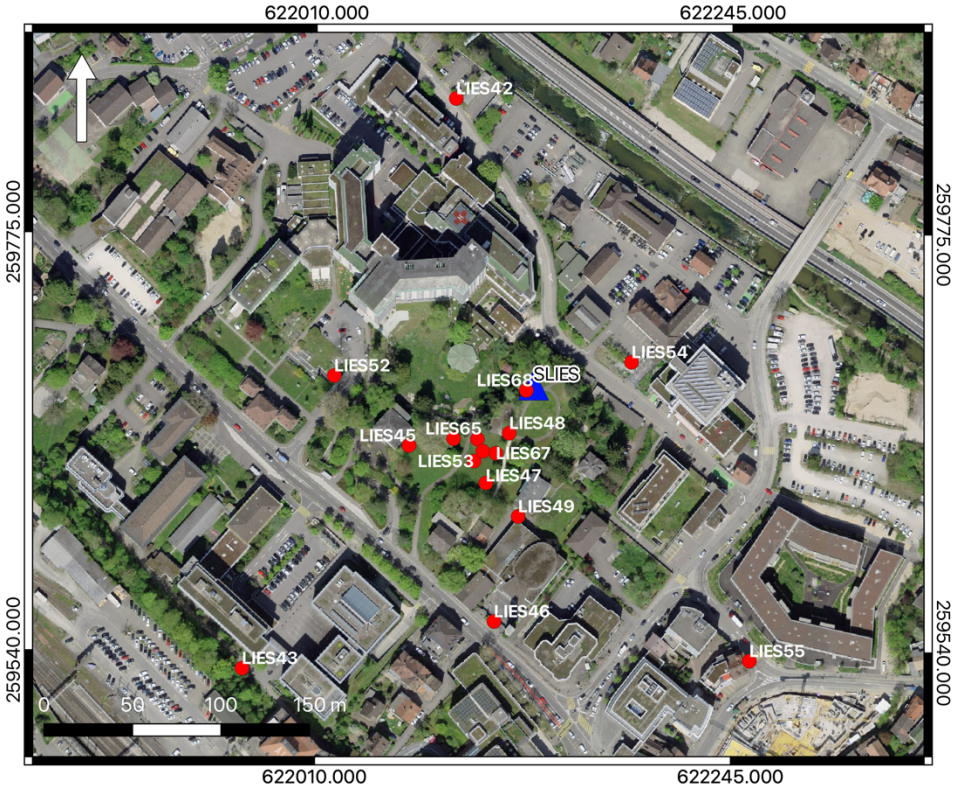

Figure 4: Layout of the array measurement in Liestal. The locations of the stations for the passive seismic measurement are indicated by the red dots. The blue triangle indicates the seismic station site. Source: Federal Office of Topography.

3.2 H/V and RayDec ellipticity curves

Figure 5 shows the H/V curves determined with the time-frequency analysis method (Fäh et al., 2009) and the RayDec ellipticity curves (Hobiger et al., 2009) for all stations of the passive array. With the exception of one curve (LIES49), the H/V curves show similar shape over the entire frequency range with two peaks divided by a central and wide trough. At low frequency, at about 1.0 Hz, one broad peak with amplitudes between 1.1 and 2.8 was picked at 10 sites (blue crosses). The second peak at about 6.4 Hz and amplitude of about 1.2-1.5 was picked at all sites (red crosses). Towards north-west and north, the frequency of the second peak increases up to 7.2 and 9.7 Hz, respectively. Fig. 6 shows the lateral variability of the peak at low frequency interpreted as the fundamental H/V peak (left) and of the other peak at higher frequencies classified as first higher mode (right).

The RayDec technique (Hobiger et al., 2009) is meant to eliminate the contributions of other wave types than Rayleigh waves and give a better estimate of the ellipticity. The RayDec ellipticity curves for all stations of the array measurements are shown in Figure 5 (right plot). These show a pattern similar to the H/V curves with two peaks divided by a central trough. The dark green curve indicates the RayDec ellipticity for the array central station (LIES64), while the dark red curve shows the ellipticity for LIES68, the closest station to SLIES permanent station.

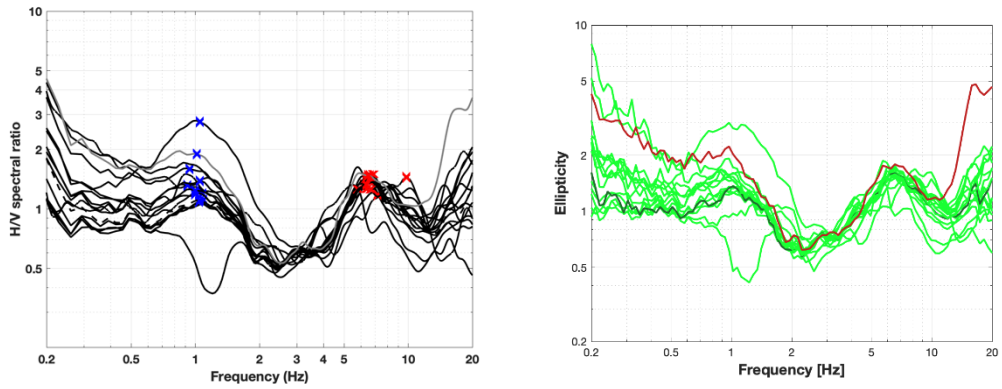

Figure 5: Left: H/V curves of the different stations of the array measurements in Liestal with picked fundamental frequency (red cross) and the first higher mode (blue cross). The dashed black curve corresponds to the center of the array (LIES64); the gray curve is the station close to station SLIES (LIES68). Right: RayDec ellipticities for all stations of the array. The curve of LIES64, the array center, is highlighted in dark green, whereas the curve of LIES68, linked to the measurement nearby the station SLIES is highlighted in dark red.

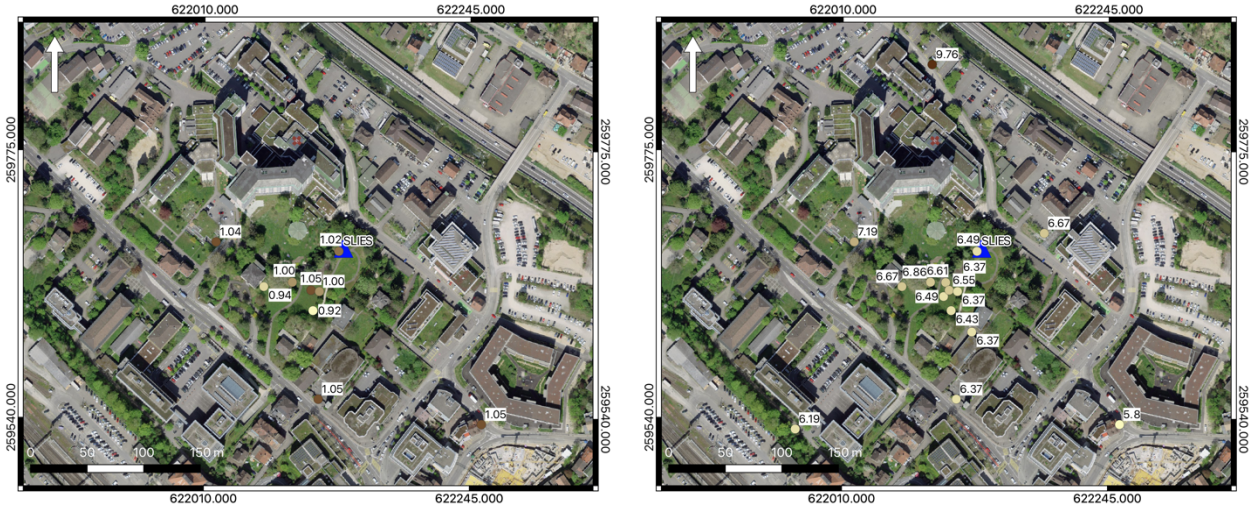

Figure 6: Map showing the variation in frequency for the H/V fundamental peak (left) and first higher mode peak (right) over the area of Liestal. Source: Federal Office of Topography.

3.3 Polarization measurements

The polarization analysis was performed according to Burjánek et al. (2010) and Burjánek et al. (2012). Fig. 7 shows the results of polarization analysis for the array center (LIES64) and the seismic station close to the station SLIES (LIES68), top and bottom rows respectively.

The ground motion of station LIES64 is elliptical over the entire frequency range and horizontal polarized at about 8 Hz and between 25 and 30 Hz (Fig. 7 – top row left and central plots); at LIES68, the ground motion is elliptical between 3 and 5 Hz changing into quasi-linear at lower and higher frequencies (Fig. 7 – bottom row left and central plots). Moreover, the ground motion at LIES68 is horizontally polarized over a wide frequency range with two peaks at about 8 Hz and between 15 and 30 Hz. For all stations located in the center and in the northern sectors, a weak direction of polarization northwest-southeast can be seen at around 3 Hz (Fig. 7 – right column); moving south, the preferential direction of polarization disappears.

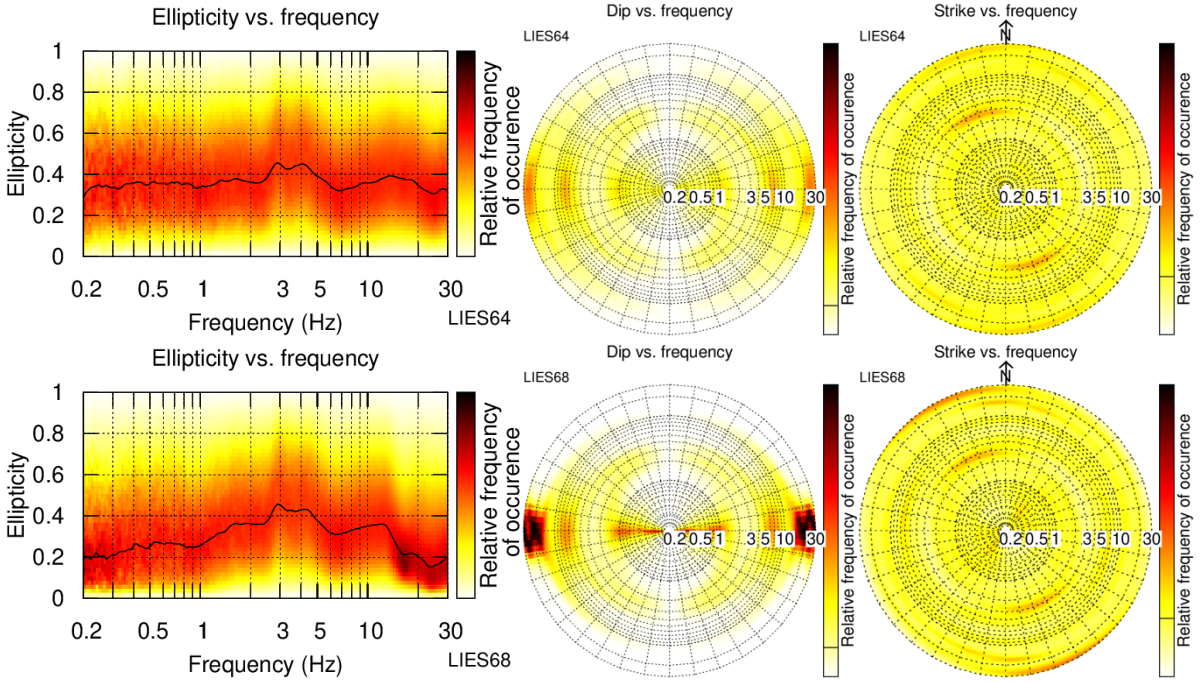

Figure 7: Polarization analysis of stations LIES64 (top line) and LIES68 (bottom line).

3.4 3-component high-resolution FK

The results of the 3-component high-resolution FK analysis (Poggi and Fäh, 2010) are shown in Fig. 8. For Love waves, using the transverse component, a continuous dispersion curve was picked between 2.80 and 48.01 Hz. For Rayleigh waves, two dispersion curves were picked using the vertical (2.45-27.95 Hz) and radial (2.66-30.31 Hz) components. The curve picked using the vertical component is continuous over the entire frequency range and shows a wide portion of the dispersion curve (4–11 Hz) with constant S-wave velocity (about 1000 m/s). At higher frequencies, a pronounced change in velocity occurs up to about 28 Hz. The curve picked for the radial component is discontinuous but shows a shape comparable to the dispersion curve picked for the vertical component.

Over the same frequency range of the two dispersion curves picked for the Rayleigh waves, two ellipticity curves with a similar trend were picked. These show two broad peaks divided by a narrow trough at about 12.8 Hz (Fig. 8 – right column).

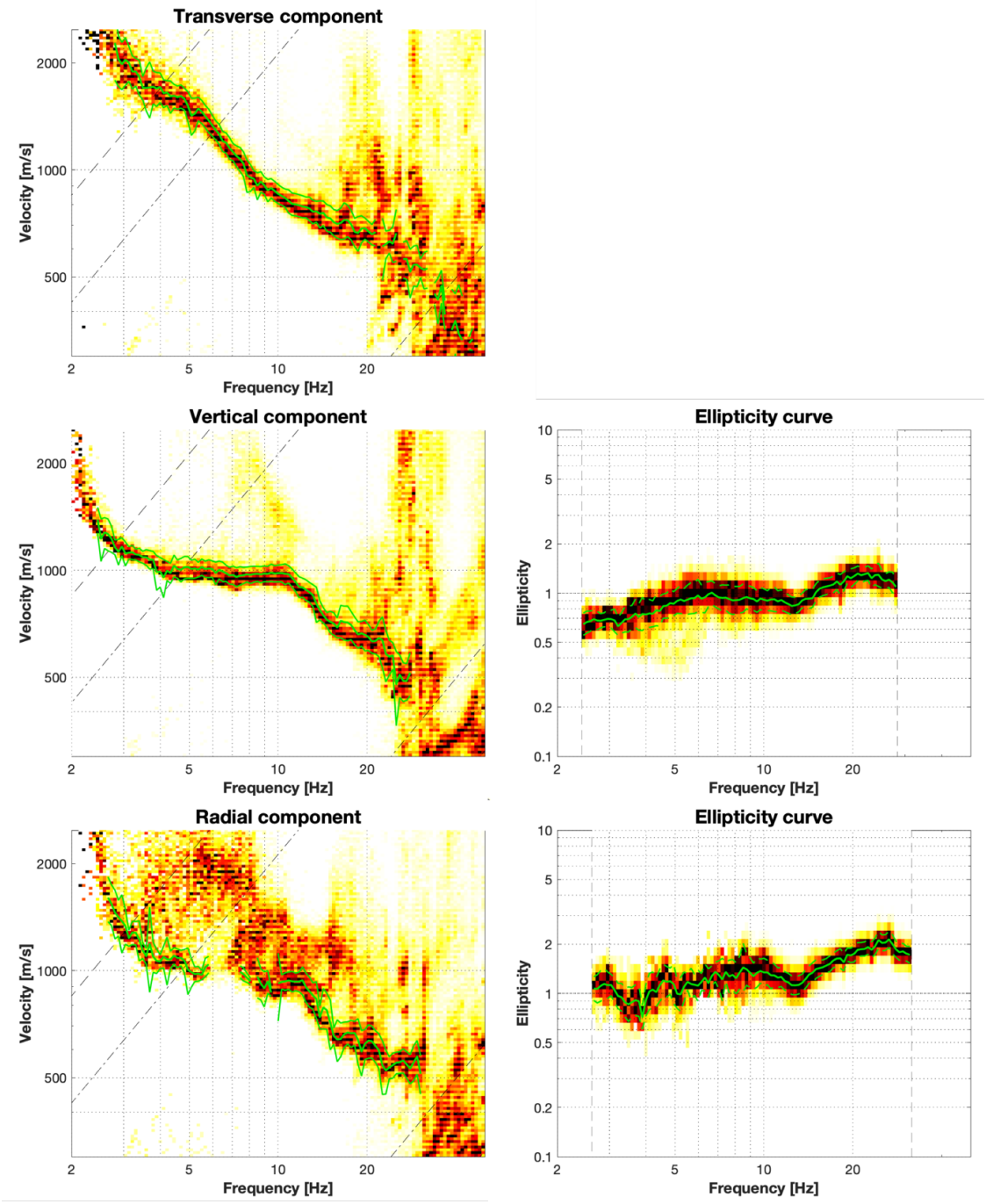

Figure 8: Left column: dispersion curves for the transverse (top row), vertical (middle row) and radial (bottom row) components. Right column: ellipticity curves for the vertical (middle right) and radial (bottom right) components obtained with the 3-component HRFK algorithm (Poggi and Fäh, 2010). The dashed and dotted black lines are the array resolution limits. The solid and dashed green lines represent the data picking (central line) and the standard deviation (outer lines).

3.5 WaveDec

The results of the WaveDec (Maranò et al., 2012) processing are shown in Fig. 9. This technique estimates the properties of single or multiple waves simultaneously with a maximum likelihood approach. In order to get good results, the parameter γ must be tuned to modify the sharpness of the wave property estimation between purely maximum likelihood estimation and a Bayesian Information Criterion. Here, a value of $\gamma = 0.5$ was used, corresponding to a 50% of Bayesian Information Criterion estimation and a 50% of maximum likelihood estimation.

The picking of dispersion curves in WaveDec was performed in the wavenumber-frequency domain and it is here shown in the velocity-frequency domain. The curve picked for the Love waves stretches between 3.18 and 20.38 Hz, while the dispersion curve picked for the Rayleigh waves goes from 2.16 to 19.51 Hz. Over the same frequency range as the dispersion curve picked for the Rayleigh wave, the ellipticity angle curve was picked. It, shown in the bottom line of Fig. 9, presents negative values for the ellipticity angle corresponding to a retrograde particle motion over the entire frequency range. At low frequencies, at about 2 Hz, the ellipticity values increase close to zero.

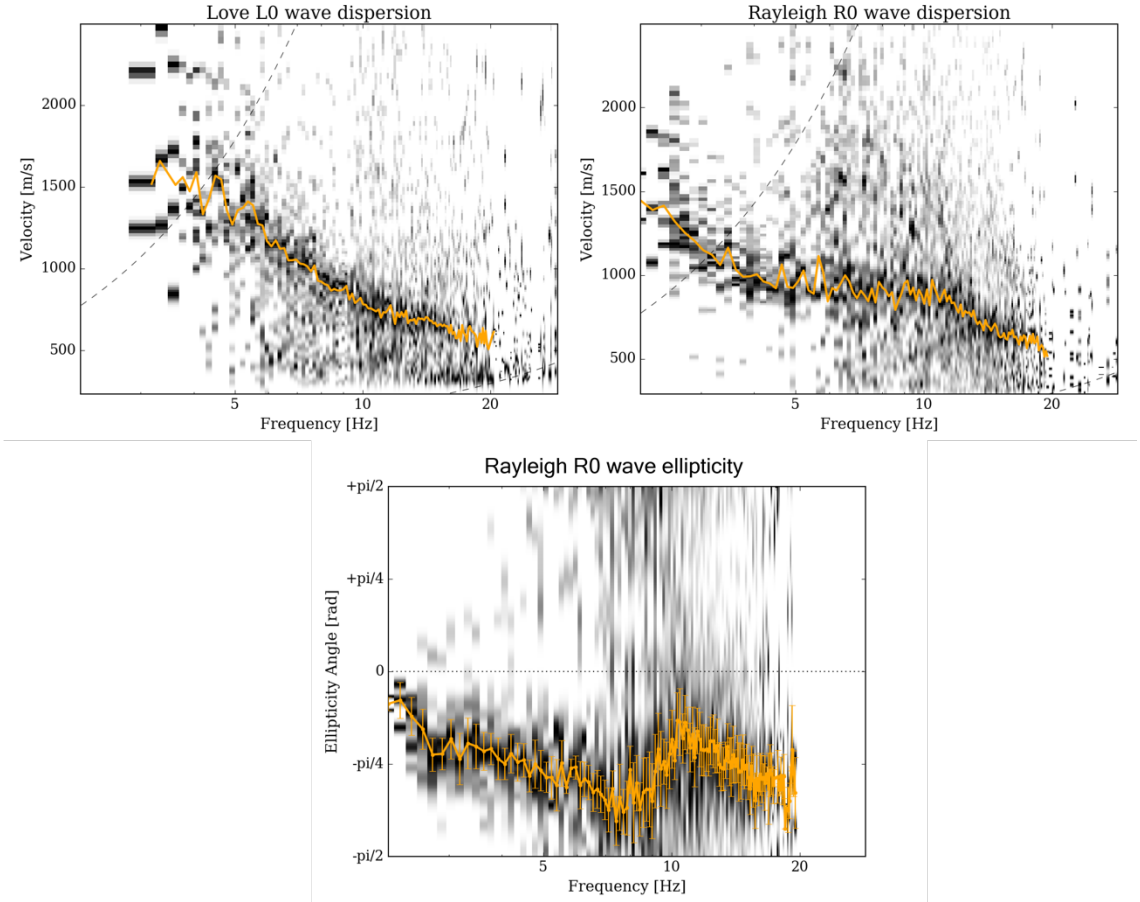

Figure 9: Dispersion curves for Love and Rayleigh waves (top row) and ellipticity angle curves for Rayleigh waves (bottom row) as obtained with WaveDec (Maranò et al., 2012). The dashed black lines (top rows) represent the array resolution limits, the solid orange line indicates the picked curve and the vertical bars at each frequency show the standard deviation for the ellipticity angle curves.

3.6 Modified SPatial AutoCorrelation

The SPAC (Aki, 1957) curves of the vertical components have been calculated using the MSPAC (Bettig et al., 2001) technique implemented in geopsy. Rings with different radius ranges are defined and for all stations pairs with distances inside this radius range, the cross-correlation is calculated in different frequency ranges. These cross-correlation curves are averaged for all station pairs of the respective ring and give the SPAC curves. The rings are defined in such a way that at least three station pairs contribute and that their connecting vectors have a good directional coverage.

The SPAC Autocorrelation curves are shown in Fig. 10 for all selected rings (central and right columns). The black points indicate the data values which contributed to the final dispersion curve estimation, which was picked using *spac2disp* of the geopsy. One dispersion curve was picked for the Rayleigh waves between 1.74 and 20.94 Hz (Fig. 10 – left).

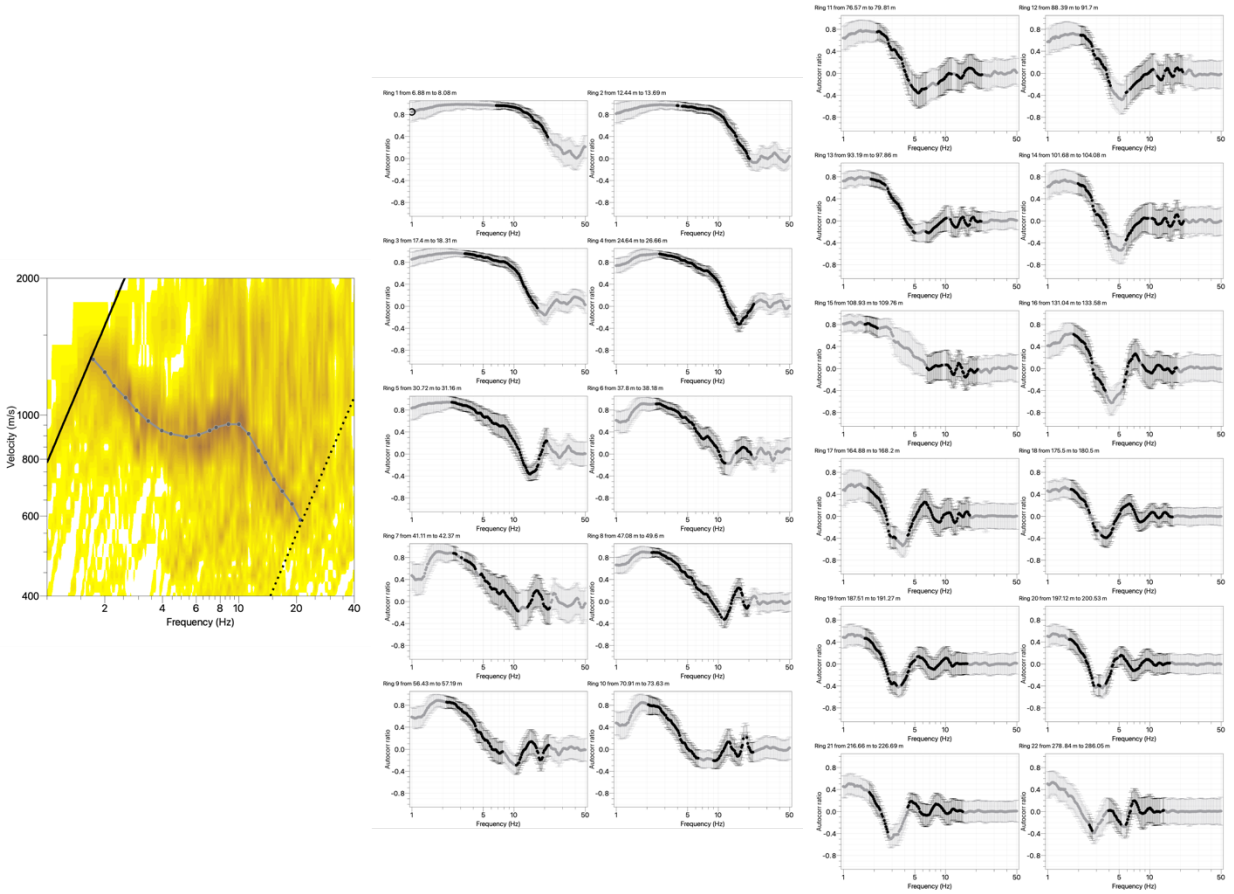

Figure 10: Rayleigh wave dispersion curve (left) obtained using spac2disp module of geopsy and autocorrelation functions for all rings (center and right). The solid gray line represents the picked data; the black dashed and dotted lines indicate the array resolution limits.

3.7 Summary

Figure 11 gives an overview of the Love and Rayleigh wave dispersion curve (left and central plots, respectively) and of the Rayleigh wave ellipticity curve (right plot) determined using different approaches. For Love waves, WaveDec and 3C-HRFK techniques produce equal dispersion curves in a frequency range between 3 and 20 Hz. For the Rayleigh waves, two dispersion curves were picked using the 3C-HRFK technique for the vertical and radial components, one using WaveDec and one using MSPAC. All these curves overlap at frequencies above 4 Hz, while at lower frequencies, small variations can be seen.

The ellipticity curves retrieved using the RayDec single station method and the array techniques are shown in Fig. 11 (right plot). The two RayDec curves are shown in the frequency range 0.2-20 Hz for the station LIES64 (array center) and LIES68 (station close to SLIES). The remaining ellipticity curves were picked for the vertical and radial components of 3C-HRFK and WaveDec technique. This curve is obtained converting the ellipticity angle curve to ellipticity.

The two RayDec curves show similar shapes between 1.5 and 10 Hz. At lower and higher frequencies, the RayDec curve for the array center (LIES64) shows much higher ellipticity values than the ellipticity curve for station LIES68. The WaveDec curve, in light blue, shows one peak and one trough; the peak is in agreement with both RayDec curves, while the trough matches only the RayDec curve for LIES68.

The two curves picked using 3C-HRFK have wide peaks, at frequencies comparable with the peaks in other ellipticity curves.

Assuming that the peak at low frequency in the RayDec curves corresponds to the fundamental H/V peak (f_0), then the first peak in the 3C-HRFK ellipticity curves and the peak in the WaveDec curve are interpreted as the first higher mode H/V peak (f_1); the remaining peak in the 3C-HRFK ellipticity curves at about 20 Hz corresponds to the second higher mode (f_2).

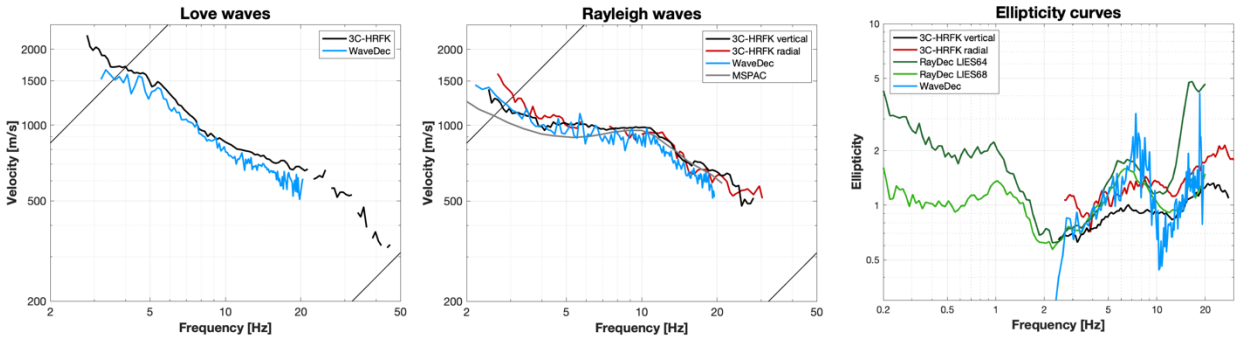

Figure 11: Comparison between the computed Love (left) and Rayleigh (center) wave dispersion curves and ellipticity curves (right).

4 Data inversion

4.1 Inversion targets

We performed several inversions using the available information. The details of the inversion targets are indicated in Table 1 and the corresponding curves are shown in black in Fig. 12.

In the inversion process, we inverted three dispersion curves and the Rayleigh wave ellipticity curve. The dispersion curves were picked using 3C-HRFK and are interpreted as follows: fundamental and first higher modes of Love waves (Fig. 12 – left plot) and fundamental mode of

Rayleigh wave (Fig. 12 – center plot). The ellipticity curve is the result of RayDec method for the LIES68 station.

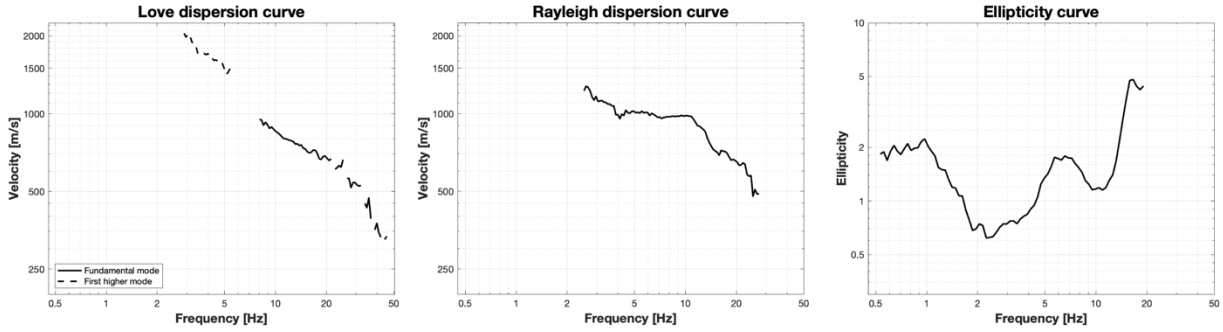

Figure 12: Overview of the dispersion curves used as target for the different inversions.

Table 1: List of the curves used as target in the inversion.

Method	Wave type	Mode	Curve type	Frequency range [Hz]
3C-HRFK	Love	fundamental	dispersion	7.95-46.02
3C-HRFK	Love	first	dispersion	2.88-5.51
3C-HRFK	Rayleigh	fundamental	dispersion	2.50-27.70
RayDec (LIES68)	Rayleigh	fundamental	ellipticity	0.52-19.15

4.2 Inversion parameterization

For the inversion, five different parameterizations were tested. The first four involve free values of thickness and velocities for the different layers, ranging from three to nine layers over the half-space. The S- and P-wave velocities are allowed to range from 50 to 3500 m/s and from 100 to 7500 m/s, respectively. The deepest layer interfaces were allowed to range to a depth of 360 m for all parameterizations. The density was fixed to 2300 kg/m^3 for the bedrock layer and to 2000 kg/m^3 for all the other layers.

The last parametrization (*SLIES fix*) had fixed layer thicknesses and consists of 20 layers over the half-space, with the deepest interface at 360 m depth. Equal ranges were defined for the P- and S-wave velocities. The density of the fix layers parametrization gradually increases from the surface to the bedrock starting at 2000 kg/m^3.

4.3 Inversion results

We performed 5 inversions with different parameterizations (see Table 2) using the Dinver routine (http://www.geopsy.org/). Each inversion run produced a total of 280000 models to assure a good convergence of the solution. The results of these inversions are shown in Figs. 13 – 17.

Table 2: List of inversions

Inversion	Number of layers	Number of models	Minimum misfit
SLIES 3l	3	280000	0.474
SLIES 5l	5	280000	0.456
SLIES 7l	7	280000	0.460
SLIES 9l	9	280000	0.472
SLIES fix	20	280000	0.443

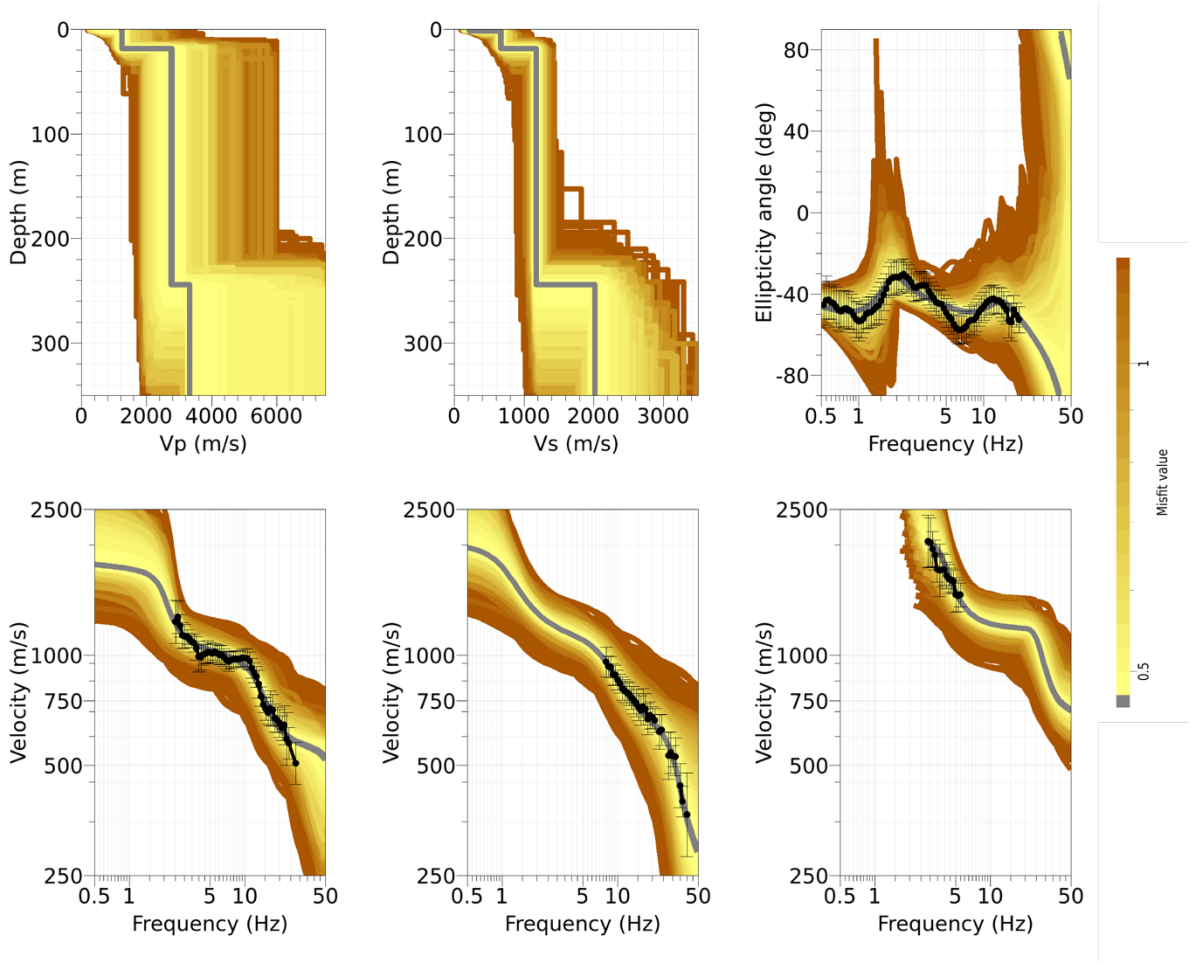

Figure 13: Inversion SLIES 3l. Top line: P-wave velocity profiles (left), S-wave velocity profiles (center) and Ellipticity angle (right). Bottom line: Dispersion curves for the fundamental mode of Rayleigh wave (left); fundamental and first higher modes of Love waves (center and right). The black dots indicate the data points used for the inversion, the black bars the standard deviation of the inverted curve, while the gray line shows the best-fitting model.

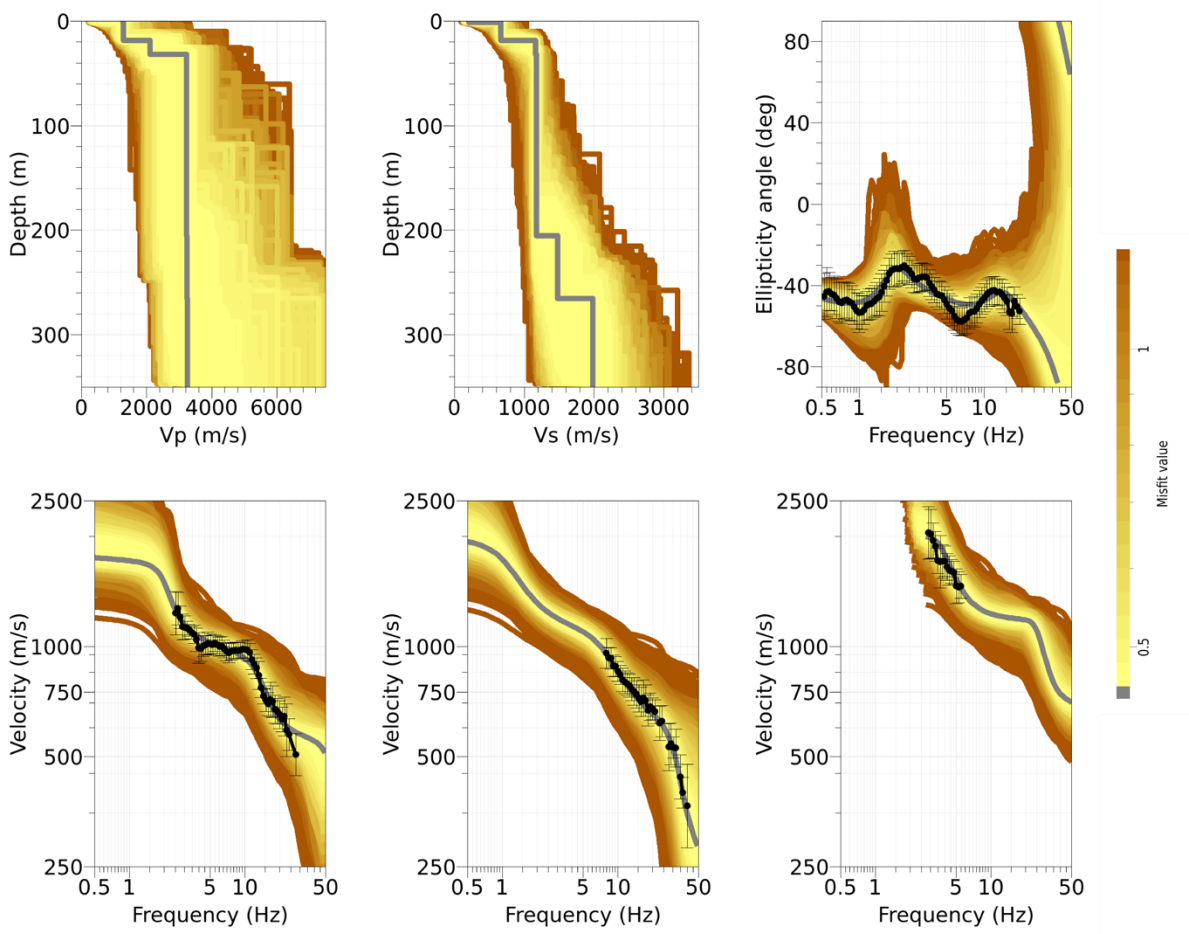

Figure 14: Inversion SLIES 5l. Top line: P-wave velocity profiles (left), S-wave velocity profiles (center) and Ellipticity angle (right). Bottom line: Dispersion curves for the fundamental mode of Rayleigh wave (left); fundamental and first higher modes of Love waves (center and right). The black dots indicate the data points used for the inversion, the black bars the standard deviation of the inverted curve, while the gray line shows the best-fitting model.

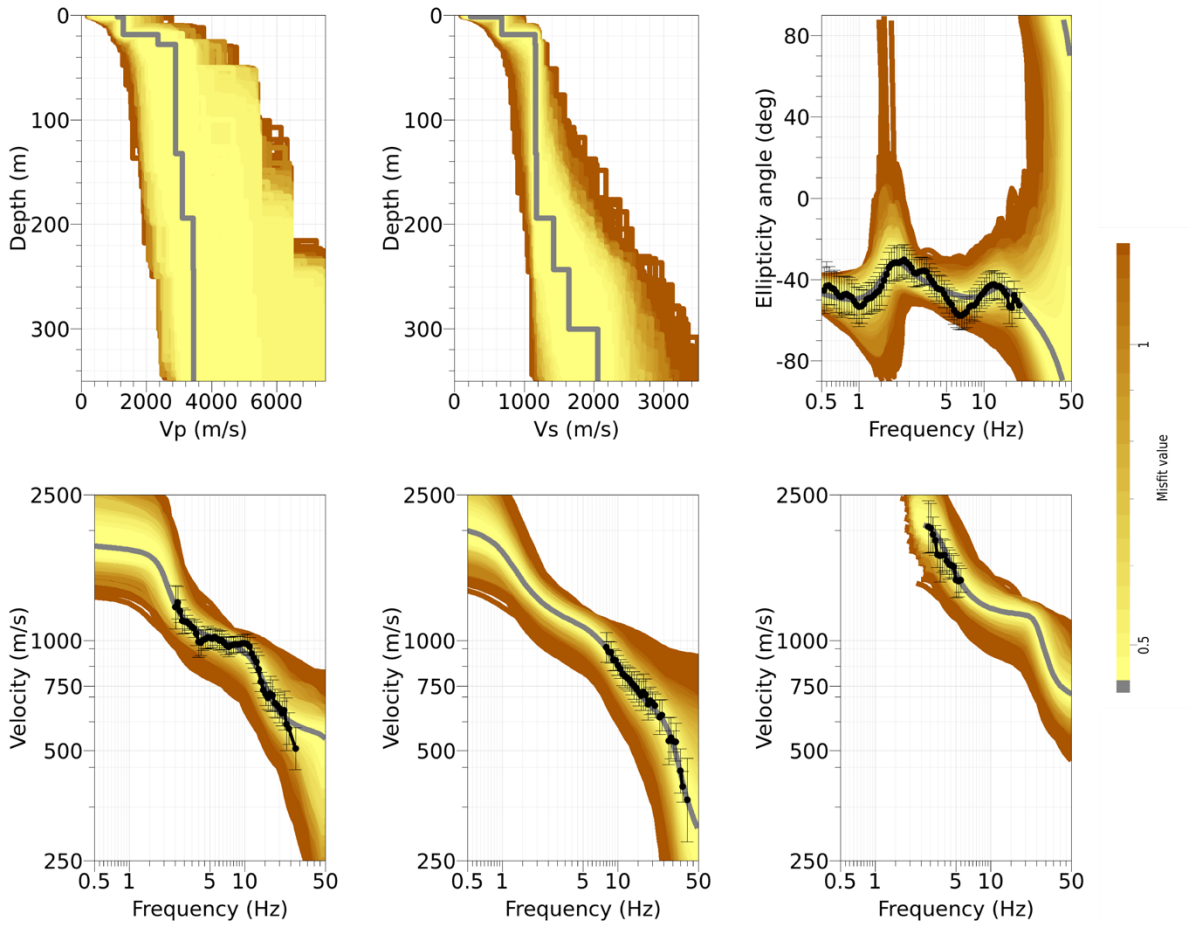

Figure 15: Inversion SLIES 7l. Top line: P-wave velocity profiles (left), S-wave velocity profiles (center) and Ellipticity angle (right). Bottom line: Dispersion curves for the fundamental mode of Rayleigh wave (left); fundamental and first higher modes of Love waves (center and right). The black dots indicate the data points used for the inversion, the black bars the standard deviation of the inverted curve, while the gray line shows the best-fitting model.

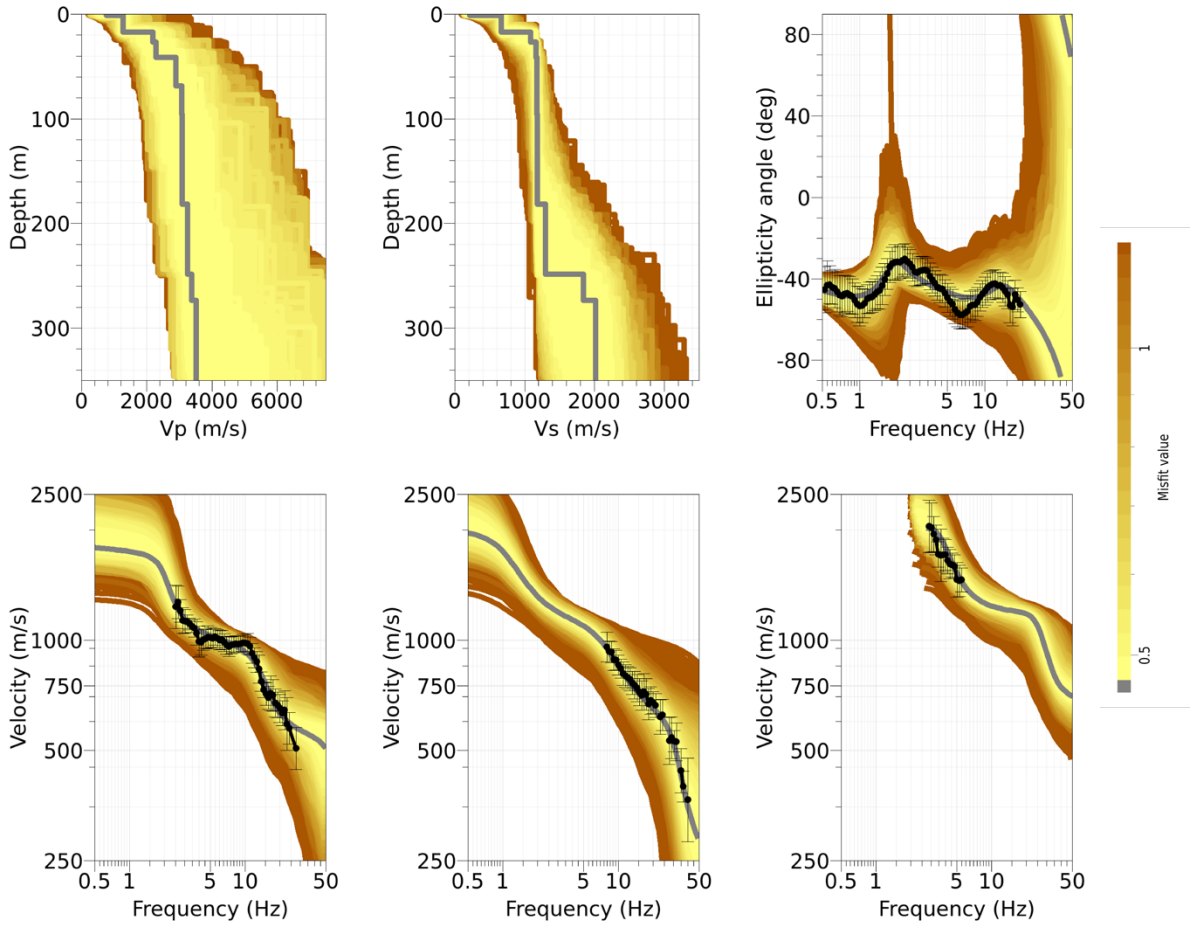

Figure 16: Inversion SLIES 9l. Top line: P-wave velocity profiles (left), S-wave velocity profiles (center) and Ellipticity angle (right). Bottom line: Dispersion curves for the fundamental mode of Rayleigh wave (left); fundamental and first higher modes of Love waves (center and right). The black dots indicate the data points used for the inversion, the black bars the standard deviation of the inverted curve, while the gray line shows the best-fitting model.

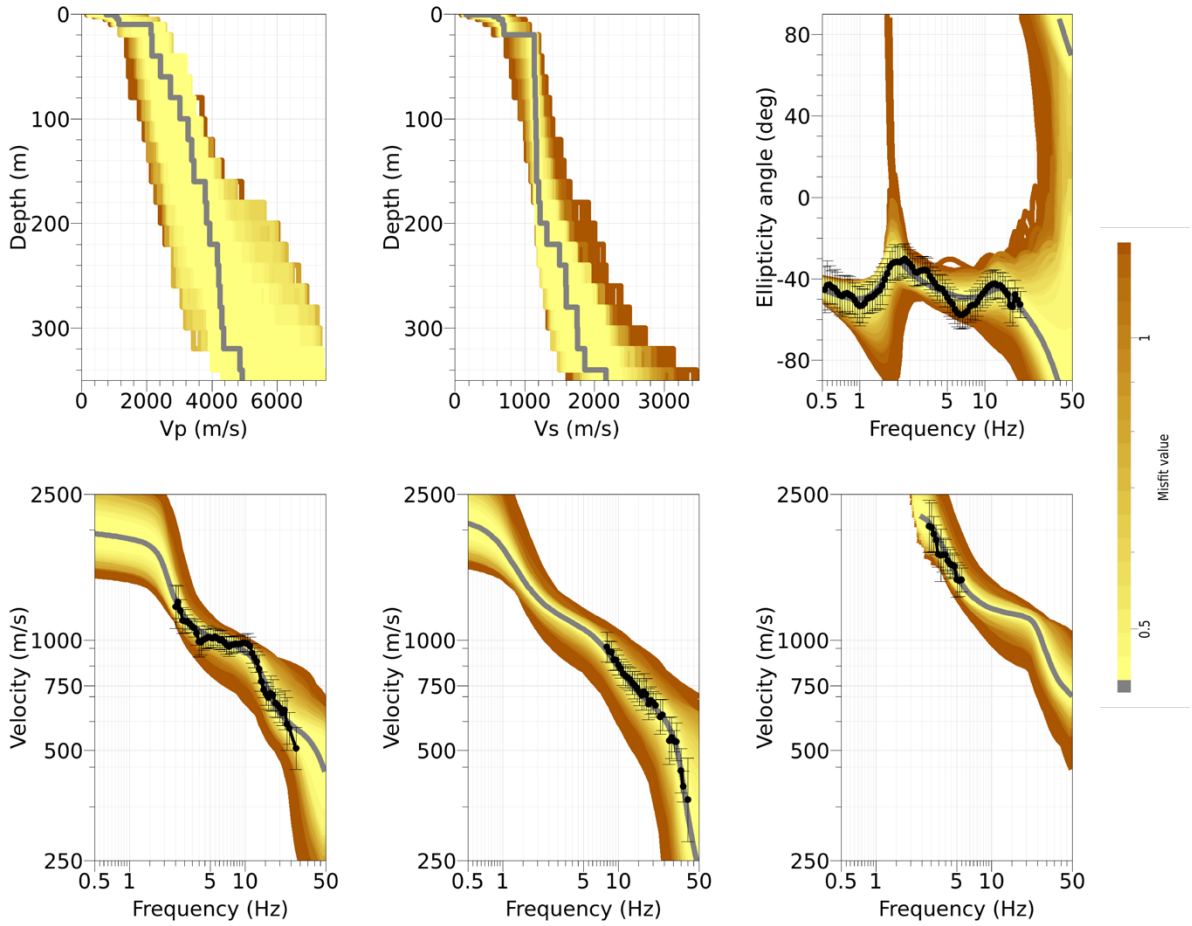

Figure 17: Inversion SLIES fix. Top line: P-wave velocity profiles (left), S-wave velocity profiles (center) and Ellipticity angle (right). Bottom line: Dispersion curves for the fundamental mode of Rayleigh wave (left); fundamental and first higher modes of Love waves (center and right). The black dots indicate the data points used for the inversion, the black bars the standard deviation of the inverted curve, while the gray line shows the best-fitting model.

4.4 Discussion of the inversion results

The best-fitting models from each inversion are shown in Fig. 18 down to 350 meters (left plot) and to 30 meters (right plot). Of all inversions performed using the same parametrization and targets, the best models are the velocity profiles with the lowest misfit.

In the first 30 meters, all velocity profiles show two interfaces: the first is at around 1.5 m and has S-wave velocity of about 665 m/s, while the second at 18.5 m shows S-wave velocities of 1156 m/s. A third interface, corresponding to the bedrock, is located at about 245 m and S-wave velocities of 2020 and 1843 m/s for *SLIES 3l* and *SLIES 9l*, respectively. The same interface is recognized in *SLIES 7l* at 265 m for S-wave velocity of about 1987 m/s. In *SLIES 5l*, there is no strong velocity contrast ascribable to the bedrock but just a gradual increase in S-wave velocity with depth.

The velocity profile obtained using the fix layers parametrization (*SLIES fix*) shows a constant increase of velocity with depth. This profile reproduces the two shallow interfaces at 1 and 20 meters and the thick layer of 140 meters with S-wave velocity of about 1173 m/s. Below this layer, a gradual increase in S-wave velocity and no strong velocity contrast can be seen down to 350 m.

The velocity profiles resulting from the different inversions have V_{S30} between 694.5 and 715.3 m/s, with an average value of 708.7 ± 8.4 m/s.

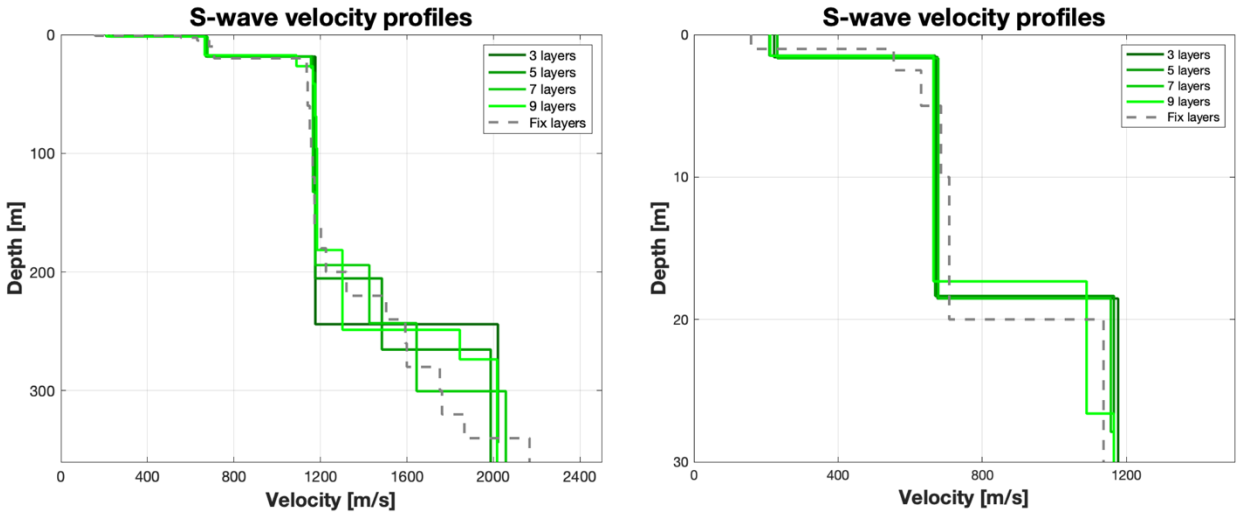

Figure 18: Overview of the best shear-wave velocity profiles of the different inversions (left) and zoom on the upper 30 m of the inversion profiles.

5 Further results from the inverted profiles

5.1 SH transfer function

In Figure 19, the average theoretical shear-wave transfer function for the best models of all parametrizations and the empirical amplification at station SLIES are shown. For the investigated site, the models predict an amplification included between 1 and 2.4 in the frequency range 0.5 – 20 Hz. Above 20 Hz, the SH-wave transfer function shows an increase in amplification values up to 4.4 at about 25 Hz. The present (05.07.2021) empirical amplification has a maximum of 8 earthquakes in the frequency range 0.79 and 6.59 Hz decreasing to 1 above 19.2 Hz. Even if the number of recorded earthquakes is low, comparable shapes can be recognized between the SH-

wave transfer function and the empirical function. Unfortunately, the fit is not perfect and the empirical amplification has values lower than the computed SH-wave curve.

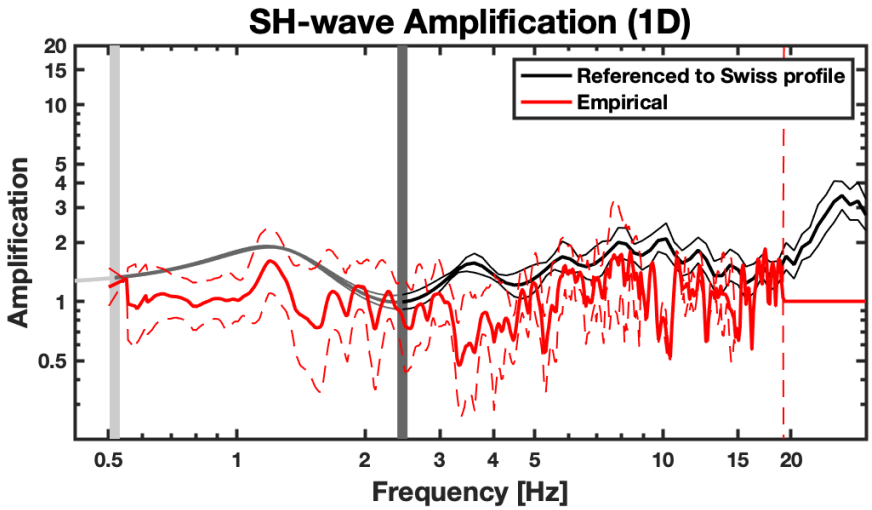

Figure 19: Modeled amplification function and standard deviation (black lines). Red curves represent the empirical amplification (solid line) and its standard deviation (dashed lines) function at the station SLIES.

5.2 Quarter-wavelength representation

The quarter-wavelength velocity approach (Joyner et al., 1981) provides, for a given frequency, the average velocity at a depth corresponding to 1/4 of the wavelength of interest. Figure 20 shows the quarter-wavelength results for the best models of all five parametrizations using the fundamental mode of Rayleigh wave dispersion curve, the fundamental and the first higher modes of Love wave dispersion curves and the Rayleigh wave ellipticity angle. The results using this proxy, considering frequency limits of the experimental data between 2.5 to 45.5 Hz for the dispersion curves and between 0.5 and 19.1 Hz for the ellipticity curve, is well constrained down to about 120 m using the dispersion curves and about 750 m using the ellipticity curve. The quarter-wavelength impedance contrast introduced by Poggi et al. (2012) is also displayed in the figure. It corresponds to the ratio between two quarter-wavelength average velocities, respectively from the top and the bottom part of the velocity profile, at a given frequency.

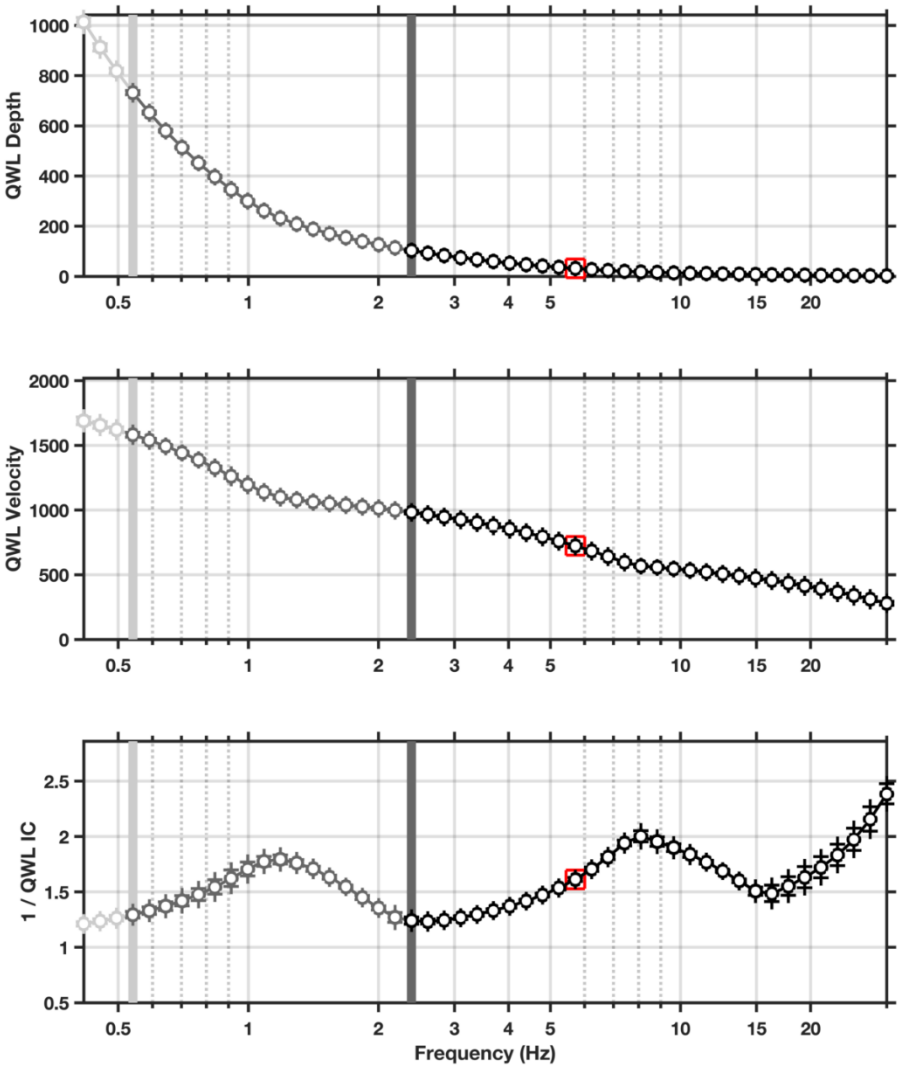

Figure 20: Quarter wavelength representation of the velocity profiles for the best models of the inversions (top: depth, center: velocity, bottom: impedance contrast). The grey light bar shows ellipticity lower frequency value, dark grey bar indicates lower frequency value obtained with dispersion curves and red square corresponds to f_{30} (frequency related to the depth of 30 m).

6 Discussion and conclusions

The passive array measurement performed in Liestal in June 2021 allowed the investigation of the subsurface underneath the station SLIES.

The H/V analysis shows a homogeneous underground with two stable peaks at 1.0 and 6.4 Hz; these peaks correspond to the main velocity contrasts and are interpreted as fundamental and first higher mode H/V peaks. Similar results were obtained using the RayDec curves as shown in the right plot of Fig. 5.

The inversion of Rayleigh and Love wave dispersion curves and of the Rayleigh ellipticity curve yields to the estimation of P- and S-wave velocity profiles investigating the subsurface down to 350 m. All velocity profiles show two shallow interfaces at 1.5 and 18.5 meters. The third interface corresponding to the transition to the bedrock is identified by the velocity profiles with 3, 7, and 9 layers between 245 and 265 meters. The velocity profile with 5 layers (*SLIES 5l*) and the profile with fix thickness layers (*SLIES fix*) do not show a velocity contrast but a gradual increase of S-wave velocity with depth.
The average V_{S30} value of the site is 708.15 m/s, corresponding to soil class B in EC8 and SIA261 classifications.
The theoretical shear-wave transfer function predicts an amplification between 1 and 2.4 in the frequency range 0.5-20 Hz with an increase up to 4.4 at 25 Hz. The theoretical shear-wave transfer function was compared with the empirical amplification observed at station SLIES, showing a good agreement in terms of shape but lower amplification.

References

Burjánek, J., Gassner-Stamm, G., Poggi, V., Moore, J. R., and Fäh, D. (2010). Ambient vibration analysis of an unstable mountain slope. Geophys. J. Int., 180:820–828.

Burjánek, J., Moore, J. R., Molina, F. X. Y., and Fäh, D. (2012). Instrumental evidence of normal mode rock slope vibration. Geophys. J. Int., 188:559–569.

Fäh, D., Gardini, D., et al. (2003). Earthquake Cataloque of Switzerland (ECOS) and the related macroseismic database. Eclogae geol. Helv. 96.

Fäh, D., Wathelet, M., Kristekova, M., Havenith, H., Endrun, B., Stamm, G., Poggi, V., Burjanek, J., and Cornou, C. (2009). Using ellipticity information for site characterisation. NERIES deliverable JRA4 D4, available at http://www.neries-eu.org.

Fritsche, S., Fäh, D., Gisler, M., and Giardini, D. (2006). Reconstructing the damage field of the 1855 earthquake in Switzerland: historical investigations on a well-documented event Geophys. J. Int. (2006)166, 719–731

Hobiger, M., Bard, P.-Y., Cornou, C., and Le Bihan, N. (2009). Single station determination of Rayleigh wave ellipticity by using the random decrement technique (RayDec). Geophys. Res. Lett., 36.

Maranò, S., Reller, C., Loeliger, H.-A., and Fäh, D. (2012). Seismic waves estimation and wavefield decomposition: Application to ambient vibrations. Geophys. J. Int., 191:175–188.

Poggi, V. and Fäh, D. (2010). Estimating Rayleigh wave particle motion from three component array analysis of ambient vibrations. Geophys. J. Int., 180:251–267.

Poggi, V., Edwards, B., and Fäh, D. (2010). Characterizing the Vertical-to-Horizontal Ratio of Ground Motion at Soft-Sediment Sites. Bulletin of the Seismological Society of America, 102(6): 2741 2756.